Table of content

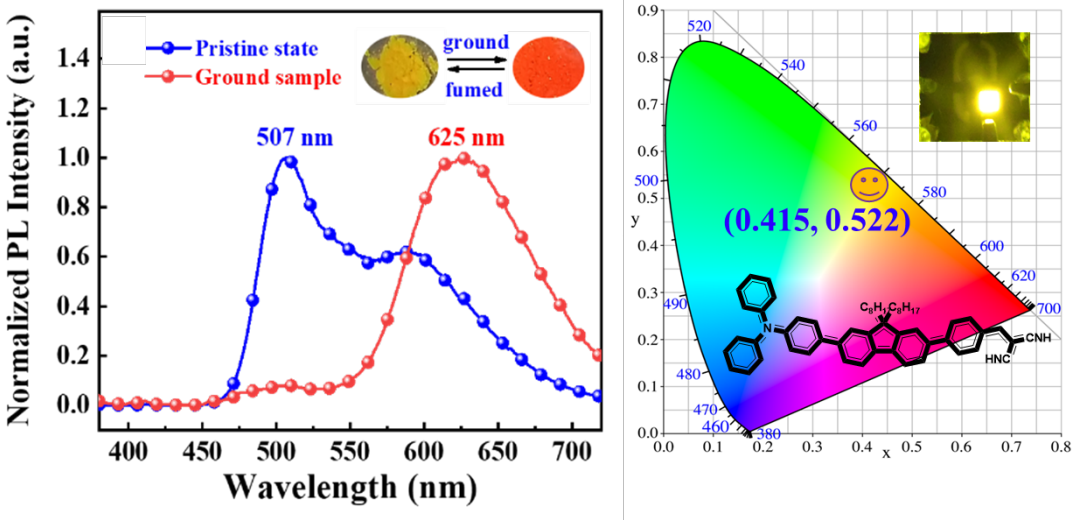

Triphenylamine-based small molecules with aggregation-induced emission and mechanochromic luminescence properties for OLED application

Xing Liu[a], Xiaozhen Wei[a], Yanqin Miao[a], Peng Tao[b,c], Hua Wang[a,*], Bingshe Xu[a,**]

[a]Key Laboratory of Interface Science and Engineering in Advanced Materials of Ministry of Education, Taiyuan University of Technology, Taiyuan, Shanxi 030024, PR China

[b]Department of Applied Biology and Chemical Technology, The Hong Kong Polytechnic University, Hong Kong, PR China

[c]The Hong Kong Polytechnic University Shenzhen Research Institute, Shenzhen, 518057, PR China

Abstract

In this work, an orange fluorescent material (**TA-DF-BDM)** with aggregation-induced emission (AIE), and mechanochromic luminescence (MCL) properties are synthesized and characterized. **TA-DF-BDM** has shown a clearer MCL with a larger emission color change from 507 to 625 nm upon mechanical grinding. On the other hand, when **TA-DF-BDM** as the emitter is applied in OLEDs, the resulting doped device exhibits excellent electroluminescent properties with the maximum luminance, CE, PE, and EQE reaching 11040 cd/m^2, 11.76 cd/A, 9.08 lm/W, and 3.89%, respectively.

Introduction

Organic luminescent materials have received considerable attention because of their potential applications in organic light-emitting diodes (OLEDs). [1-6] To achieve this real-world application, organic luminescent materials (OLMs) have been demonstrated to play important roles as emitters in OLEDs. Owing to these recent efforts in novel OLMs, a number of high-performance OLEDs have been developed, especially for those in red and green colors. [7, 8] For most conventional OLMs, impressive emissive features can be obtained in their dilute solutions, while weak or completely quenched emission was observed in the solid state for the detrimental aggregation-caused quenching (ACQ). Yin and co-workers incorporated dendrimer as an outshell to suppress the aggregation of organic chromophore and then provide the strategy to overcome ACQ problems. [9] That although impressive performance can be obtained in some cases, the complicated procedures and uncontrollable phase separation usually limit their further applications. [10-12]In 2001,Tang and his co-workers observed a unique photophysical phenomenon of “aggregation-induced emission (AIE)”.[13] Since then, AIE has been considered as one of the most powerful strategy for overcoming ACQ effect and the corresponding AIE luminogens (AIEgens) with high solid state PL efficiency are frequently used as emitters in OLEDs.[14-18] Another significant negative factor is that red and near-infrared (NIR) emitters typically show relatively low luminescence efficiency due to their large non-radiative decay rates that increase exponentially with an increase in the emission wavelength, as governed by the energy gap law.[19] Triphenylamine and its derivatives were a kind of photoelectric

materials with excellent properties, the helical structure is conducive to the construction of AIE compounds. It is also an important segment in the construction of long-wave emitting AIE compounds. Triphenylamine derivatives are widely investigated because of their superior performance such as their processibility, high fluorescent quantum yields, chemical and thermal stability in the solid state. [20] On the other hand, triphenylamine unit is a preferred electron-donating moiety with excellent hole-transporting, and tridimensional steric properties. [21]

Mechanochromic luminescent (MCL) materials appearing to change colour of fluorescent emission under external mechanical stimuli, have attracted increasing interest recently, due to their potential applications in optoelectronic devices, mechanosensors, data storage systems, and security papers [22-24]. However, efficient OLEDs based on MCL materials are still very rare. Hence, the development of multifunctional luminescent materials with MCL and AIE properties simultaneously may be of great importance both scientifically and practically.

In this work, we designed and synthesized an orange fluorescent material (**TA-DF-BDM)** with twisting D-π-A configuration, in which triphenylamine (TPA), benzylidenemalononitrile (BDM) and 9,9-dioctylfluorene serve as D, A, and the π-conjugation unit, respectively. Herein, TPA is a strong electron donor group and has a high HOMO energy level. More importantly, the molecular space of TPA exhibits a certain twist angle, which can effectively avoid the accumulation of molecules for constructing an intramolecular CT state. The 9,9-dioctylfluorene provides the necessary conjugation for the molecular backbone, ensuring the satisfactory contribution for the

improving η_{pl} of fluorescent molecules. As a consequent, the synthesized **TA-DF-BDM** exhibit good mechanochromic luminescence performance. And, when **TA-DF-BDM** as emitter is applied in OLEDs**,** the resulting doped device exhibits excellent electroluminescent properties with the maximum brightness reaching 11040 cd/m^2.

Results and Discussion

Synthesis and structure characterization

The Scheme 1 depicts the synthetic route to **TA-DF-BDM**. The synthesis started with the Suzuki coupling of 9,9-dioctyl-2,7-dibromofluorene with stannylated triphenylamine 4-borate. Next the precursor M1 undergoes suzuki coupling reaction with 4-acylphenylboronic acid to get the product M2. The final product **TA-DF-BDM** was obtained by additional reaction. The final product was purified using silica gel column chromatography. The structure and purity of the final product are fully confirmed by the ^{1}H NMR, ^{13}C NMR, mass spectrometry and elemental analysis (Fig. S1-7).

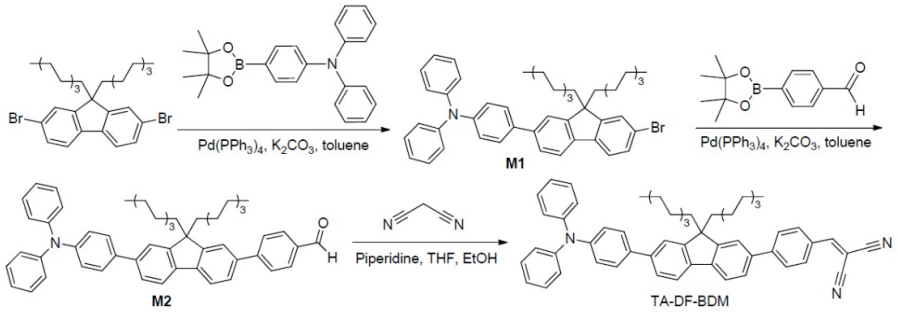

Scheme 1. Chemical structures and synthetic route of **TA-DF-BDM**

Crystal Structure

Single crystal of the compound was obtained by slow diffusion of ethanol into a methylene dichloride, and used for single crystal X-ray diffraction analysis (Table

S1). The unit cell of **TA-DF-BDM** is triclinic, space group P-1, containing four molecules. As shown in Fig. 1-a, the torsional angle between the TPA substituents and the central 9,9-dimethylfluorene was 28.51°, and the dihedral angle between benzylidenemalononitrile and central 9,9-dimethylfluorene was 28.46°, which is much smaller than that of the theoretical calculation. As presented in Fig.1-b, the N-atom of benzylidenemalononitrile and the benzylidenemalononitrile -H of the adjacent molecules form C-H…N hydrogen bonds and the length of these hydrogen bonds in the range of 2.669 Å. We concluded that the intermolecular hydrogen bonds by the cyano group are the driving force to urge the long-range order in these molecules (as shown in Fig. 1-c).

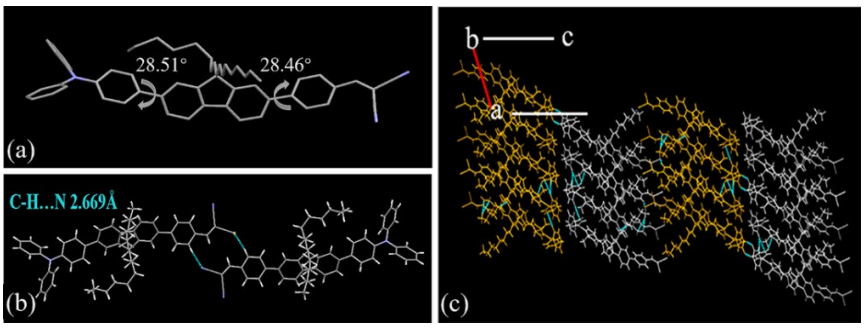

Fig. 1 The Single-crystal structure of **TA-DF-BDM**. (a) A single molecular structure of **TA-DF-BDM** crystal; (b) intermolecular interactions; (c) The stack mode of the crystal.

Theoretical Calculations

To further explore the relationship between the material property and molecular structure of **TA-DF-BDM**, the electronic structure was calculated, and optimized structures and frontier molecular orbital distributions were shown in Fig. 2. As depicted, the optimized conformation of **TA-DF-BDM** shows a twist angle of 35.6° between the TPA substituents and the central 9,9-dimethylfluorene, and the dihedral angle between benzylidenemalononitrile and central 9,9-

dimethylfluorene was 33.8°. HOMOs and LUMOs of **TA-DF-BDM** are mainly distributed on D unit of TPA and A unit of BDM, respectively. The separation of electron density distribution of HOMOs and LUMOs indicates the existence of CT state. The calculated energy levels (HOMO and LUMO) are -5.03 eV and -2.81 eV.

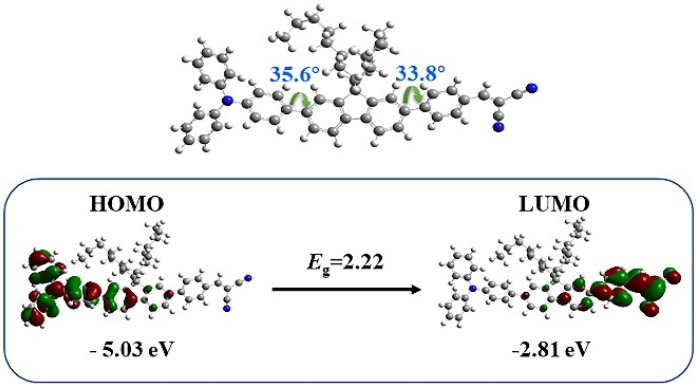

Fig. 2 Optimized structures and frontier molecular orbital distributions of **TA-DF-BDM**.

Photophysical Properties

The photophysical properties of the compound was studied by the ultraviolet-visible (UV-vis) and PL spectrum. The UV-vis absorption spectra of different solvents are shown in Figure 3 (a), and it can be seen that with the change of solvent polarity, the position of the material absorption peak hardly moves. The absorption peaks located at 305 nm and 360nm, corresponding to the n-π* transition between n electrons and π electrons on N heteroatoms of triphenylamine, and the π-π* transition of the benzene ring on the fluorene conjugated chain. The fluorescence spectra of TA-DF-BDM in different increasing solvent polarity (Fig. 3b) indicate that the emission peak (λemmax shifted 97 nm (485-582 nm)).

The UV-vis absorption spectra showed almost no change but obvious solvatochromic PL was observed on varying the solvent polarity. This is

rationalized by the fact that the excited state is more polar than the ground state. In the excited state, electrons are excited from HOMO to LUMO causing redistribution of the charge and conformational change to form an ICT state in a D-π-A material. The polarized excited state can be stabilized by the high polar solvents because the solvent molecules reorient around the molecule to lower the energy of the system thereby leading to a red shift in the emission spectra.

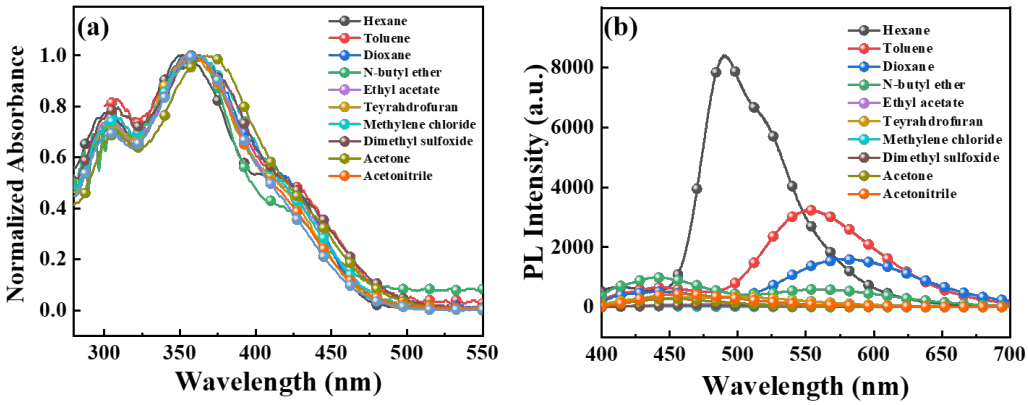

Fig. 3 (a) UV-Vis absorption and (b) PL spectra of **TA-DF-BDM** in different solvents (1.0×10^{-5} mol/L)

Triphenylamine (TPA) is a typical AIE compound. It is thus envisioned that TA-DF-BDM is also AIE active. To verify this, fluorescence spectra of TA-DF-BDM in THF and THF–water mixtures were measured. Water is chosen because it is a typical non-solvent for the compounds: the luminogen molecules must aggregate in the THF–water mixtures with high water fraction (fw). As shown in Fig. 4, TA-DF-BDM in pure THF and THF–water mixtures (fw) <80% exhibited extremely weak PL signals, which was ascribed to the active intramolecular rotations of the genuinely dissolved luminogens in these mixtures. However, when fw was increased to 80%-90%, the emission was boosted swiftly and its intensity was ca. 2.52-fold higher than that in THF. In high fw mixtures, due to

the reduction in the solvating power of the aqueous media, these molecules start to aggregate, which greatly impedes the intramolecular rotations of the molecules. It renders the excitons deactivated mainly through the radiative path, thus boosting the emission. The emission peak has different red shift. The redshift is caused by the formation of J-aggregates, the molecular arrangement tends to be planar, and the degree of conjugation increases.

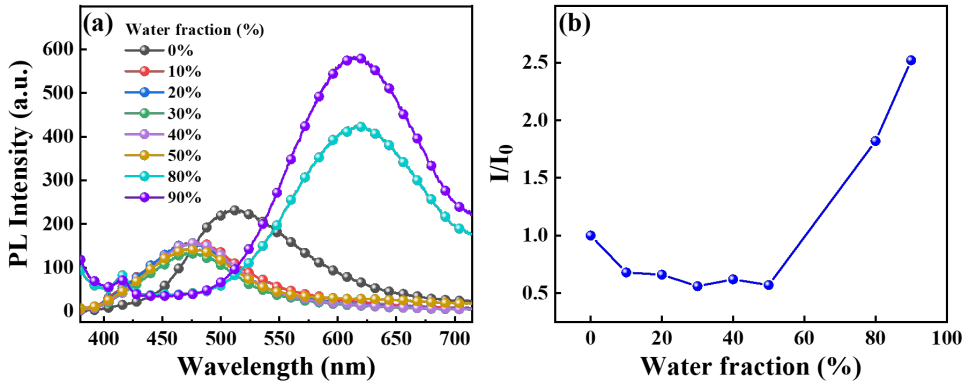

Fig. 4 (a) Fluorescence spectra of **TA-DF-BDM** in the mixtures of THF and water with different water fractions (f_w); (b) Normalized fluorescent emission intensities of **TA-DF-BDM** in THF/water with different f_w

Mechanochromic property

We previously found that some Triphenylamine compounds exhibited MFC properties and the non-planar architecture of Triphenylamine compounds as well as the ICT feature of the D-π-A system were favorable for mechano-fluorochromism.

Herein, we investigated the mechano-fluorochromic properties of these compounds and found that TA-DF-BDM gave different emitting behaviors upon the treatment of grinding and fuming. It was clear from the inset of Fig. 5 that TA-DF-BDM exhibited obvious MFC behavior. As shown in Fig. 5(a), the pristine state of TA-DF-BDM emitted bright yellow fluorescence with emission peak at

ca. 507 nm. Upon grinding using a mortar and pestle, the pristine state converted to orange fluorescence and the emission peak red-shifted to 625 nm. Moreover, the emitting color could be recovered to yellow (ca. 507 nm) after the ground powders of TA-DF-BDM were fumed with DCM. To evaluate the difference of the solid-state fluorescence behaviors between pristine crystal and amorphous states, the phase transition characteristics of TA-DF-BDM were investigated by powder X-ray diffraction (XRD). The XRD diffractograms of the pristine cryst exhibited intense and sharp reflection peaks, indicative of their well-ordered crystalline natures. In contrast, after grinding, the diffraction peaks disappeared and only a diffuse band was observed, which implied that grinding led to a crystalline to amorphous phase conversion of solids (Fig. 5b). After exposing the ground samples to DCM vapor, the sharp and intense diffraction peaks reappeared (Fig. S9). Their reappearance demonstrated that the amorphous powder restored its pristine crystallinity upon solvent fumigation. Thus, the powder XRD results revealed that the MFC mechanism of TA-DF-BDM could be ascribed to a morphological transition between crystalline and amorphous states upon the ground/fumed process. Ground induced structural transition character of TA-DF-BDM probably leaded to changes in packing, which allowed a more planar structure and perhaps better dipole-dipole intermolecular interactions, leading to a red shift of fluorescence.

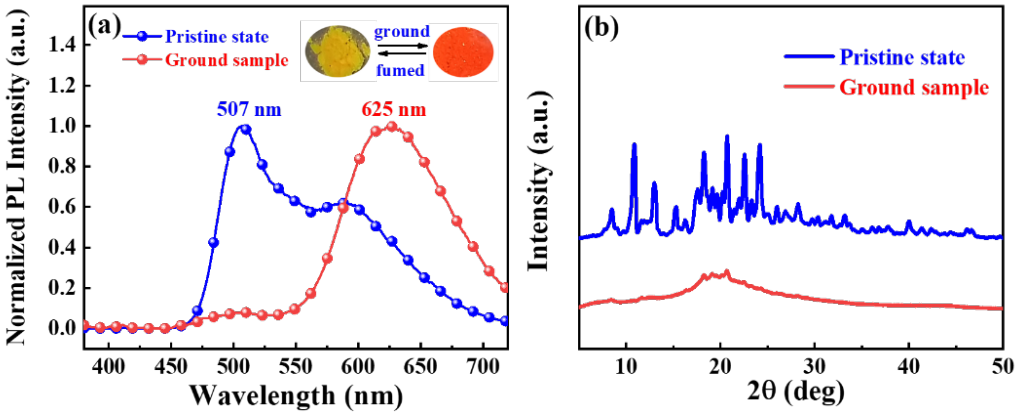

Fig. 5 (a) normalized fluorescence spectra of **TA-DF-BDM** in different solid-states:pristine and ground solids. Inset: Photos of **TA-DF-BDM** during MFC process under 365 nm light. (b) XRD patterns of **TA-DF-BDM** in pristine and ground solids

Electroluminescent Performance

To evaluate electroluminescent performance of TA-DF-BDM , we fabricated the doped OLED with TA-DF-BDM as emitter, and the detailed device configuration is ITO/MoO_3 (3 nm)/TAPC(4,4'-cyclohexylidene bis[N,N-bis(p-tolyl)aniline]) (40 nm)/TCTA(4,4',4"-Tris(carbazol-9-yl)-triphenylamine) (10 nm)/CBP (4,4'-Bis(N-carbazolyl)-1,1'-biphenyl):x wt%TA-DF-BDM (20 nm)/TPBi (1,3,5-Tris(1-phenyl-1H-benzimidazol-2-yl)benzene) (50 nm)/LiF (1 nm)/Al, where x is 2 wt%, 3 wt%, 5 wt%, and 8 wt% corresponding to device A1, A2, A3, and A4, repectively. In this device, MoO_3 and LiFe were used as the hole-injection layer (HIL) and electron-injection layer(EIL), respectively; TAPC and TPBi served as hole-transporting layer (HTL) and electron-transporting layer (ETL), respectively; TCTA served as exciton blocking layer (EBL); CBP doped DF-BDM layer served as light-emitting layer(LEL); and ITO and Al served as anode and cathode, respectively.

From the EL spectra of devices A1-A4 in Fig. 6a, it can be seen all devices

emit yellow-orange light with emission peak at range of 549 to 580 nm. It is clear with the decrease of doping concentration of TA-DF-BDM, the emission peak for corresponding device presents a blue-shift trend. This is easy to understand that the interactions between TA-DF-BDM molecules in the doped devices is obviously weaker than in the non-doped device A (Fig. S10 and Fig. 5), and with the decrease of doping concentration, the interactions become less and less, which lead to a relatively large band gap in the doped devices, further inducing a blue-shift EL spectra. From Fig. 6b-d and Table, all devices also show a relatively low turn-on voltage of 2.99~3.30 V, and with the increase of doping concentration, the turn-on voltage for corresponding device shows a decreasing tendency. This may be ascribed to the electron-transport nature of BDM and hole-transport nature of TPA units in TA-DF-BDM facilitate the charge transportation. The optimized device A3 with 5wt% TA-DF-BDM achieve the highest device efficiency with maximum current efficiency (CE), power efficiency (PE), and EQE reaching 11.76 cd/A, 9.08 lm/W, and 3.89%, respectively. And this device also realizes the high maximum luminance of 11040 cd/m^2.

Table 1. Summary of EL performance for all TA-DF-BDM –based devices

Device [a]	TA-DF-BDM (doped ratios)	λ_{EL} [nm]	EQE [b] [%]	CE_{max} [cd/A]	PE_{max} [lm/W]	L_{max} [cd/m^2]	CIE (x,y)	V_{on} [c] [V]
DeviceA1	2 wt%	549	3.64	10.53	7.39	9119	(0.379,0.500)	3.30
DeviceA2	3 wt%	550	3.79	11.20	8.55	11290	(0.400,0.520)	3.30
DeviceA3	5 wt%	556	3.89	11.76	9.08	11040	(0.415,0.522)	3.29
DeviceA4	8 wt%	580	2.80	6.32	6.82	8944	(0.480,0.495)	2.99

b) EQE_{max} = maximum external efficiency; CE_{max} =maximum current efficiency; PE_{max} =maximum power efficiency; L_{max} = maximum luminance; CIE = Commission International del'Eeclairage coordinates (1931 CIE chromaticity diagram); c) Turn-on voltage

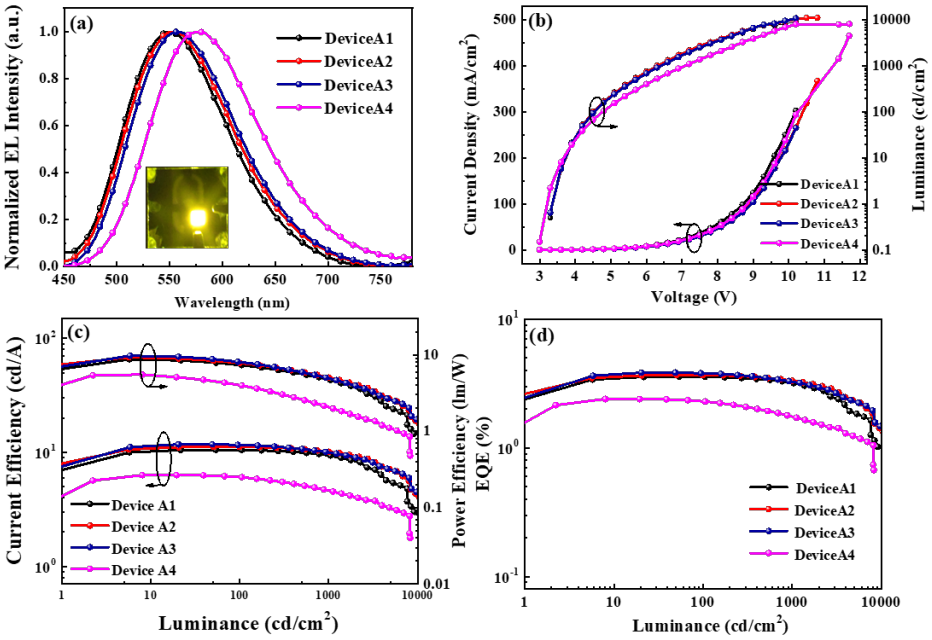

Fig. 6 EL performance (doped) of TA-DF-BDM: (a) EL spectra; Inset: Photos of DeviceA1 (b) J-V-L curves; (c) CE-L-PE curves; (d) EQE-L curves

Conclusions

In summary, an orange -emitting compound TA-DF-BDM was successfully designed and synthesized, in which triphenylamine and benzylidenemalononitrile are employed as D and A moieties, and 9,9-dimethylfluorene as the π-conjugation bridge. Both theoretical calculation and experimental results revealed that TA-DF-BDM displayed the solvatochromic effect from CT excited state. Further, TA-DF-BDM also shows reversible MFC property, where it was observed the TA-DF-BDM powder could emit intense yellow light under UV irradiation, and after grinding, the emitting colors of TA-DF-BDM would change into orange light. Moreover, the fabricated doped device with TA-DF-BDM as emitter achieved the excellent EL performance with the maximum luminance, CE, PE, and EQE reaching 11040 cd/m2, 11.76 cd/A, 9.08 lm/W, and 3.89%, respectively,

demonstrating the great potential of TA-DF-BDM in the development of high-performance yellow and white OLEDs.

Conflicts of interest

There are no conflicts to declare.

Acknowledgements

This work was financial supported by the National Natural Scientific Foundation of China (61775155, 61705156), Key R&D program of Shanxi Province (201903D121100, 201903D421087), Natural Science Foundation of Shanxi Province (201901D111108).

Supporting information

Section 1. Materials and Method

Synthetic Section

All reagents and organic solvents were purchased from commercial chemical reagent company and used without further purification. The Synthetic route of **TA-DF-BDM** is shown in Scheme 1.

(1) 4-(7-bromo-9,9-dioctylfluoren-2-yl)-N,N-diphenylaniline (M1)

The triphenylamine 4-borate (0.371 g, 1 mmol) and 9,9-dioctyl-2,7-dibromofluorene (1.192 g, 2 mmol) were dissolved in 15 mL of toluene, into which K_2CO_3 water solution (2M, 10 mL) was dropped. Then, tetrakistriphenylphosphine palladium ($Pd(PPh_3)_4$) (0.057 g, 0.05 mmol) was added into above reaction mixture. After refluxing for 4 h under nitrogen protection, the reaction mixture was poured into water and extracted with dichloromethane. The collected organic layer was dried over anhydrous $MgSO_4$ and concentrated under reduced pressure. Finally, the resultant residue was purified by silica gel column chromatography using mixture eluents of ethyl acetate and hexane (1:20, v/v), which afforded M1 as intermediate product (0.3123 g, 74.2%, $C_{47}H_{54}BrN$: C 79.22, H 7.59, Br 11.22，N 1.97; found: C 79.17, H 7.72, Br 11.22, N 1.97).

^{1}H NMR (600 MHz, DMSO) δ 7.86 (d, *J* = 7.9 Hz, 1H), 7.77 (d, *J* = 8.1 Hz, 1H), 7.72 (d, *J* = 1.3 Hz, 1H), 7.64 (ddd, *J* = 16.5, 10.7, 8.7 Hz, 4H), 7.51 (dd, *J* = 8.0, 1.8 Hz, 1H), 7.36-7.29 (m, 4H), 7.10 -7.02 (m, 8H), 2.04 (tt, *J* = 13.3, 8.3 Hz, 4H), 1.25-0.95 (m, 20H), 0.75 (t, *J* = 7.2 Hz, 6H), 0.49 (s, 4H).

(2) 4-(7-(4-(diphenylamino)phenyl)-9,9-dioctylfluoren-2-yl)benzaldehyde (M2)

The intermediate product of M1 (0.381 g, 0.5 mmol) and 4-acylphenylboronic acid (0.234 g, 1 mmol) were dissolved in 15 mL of toluene, which mixed with K_2CO_3 water solution (2 mol/L, 10 mL). Then, Pd $(PPh_3)_4$ (0.057 g, 0.05 mmol) was added into reaction mixture, which were been refluxing overnight under nitrogen protection. Then, the resulting mixture was poured into water and extracted with dichloromethane. The collected organic layer was dried over anhydrous $MgSO_4$ and concentrated under reduced pressure. Finally, the resultant residue was purified by silica gel column chromatography using ethyl acetate and hexane (1:15, v/v) as eluents to afford M2 as intermediate product (0.2308 g, 60.6%, $C_{54}H_{59}NO$: C 87.92, H 8.01, N 1.90， O 2.17; found: C 87.75, H 8.12， N 1.90, O 2.17).

^{1}H NMR (600 MHz, $CDCl_3$) δ 10.08 (s, 1H), 8.00-7.96 (m, 2H), 7.85-7.82 (m, 2H), 7.81-7.75 (m, 2H), 7.64 (dd, *J* = 7.9, 1.7 Hz, 1H), 7.61-7.54 (m, 5H), 7.30-7.27 (m, 3H), 7.26 (d, *J* = 4.3 Hz, 1H), 7.20-7.13 (m, 6H), 7.04 (tt, *J* = 7.5, 1.1 Hz, 2H), 2.08-1.98 (m, 4H), 1.21-1.00 (m, 20H), 0.78 (t, *J* = 7.2 Hz, 6H), 0.70 (t, *J* = 10.6 Hz, 4H).

(3) TA-DF-BDM

The intermediate product of M2 (0.246 g, 0.33 mmol) and malononitrile (0.066 g, 1 mmol) were dissolved into mixture solution of absolute ethanol (15 mL) and tetrahydrofuran (THF) (5 mL). The reaction mixture was keeping refluxing for 3 h. Then, the solvent was

concentrated under reduced pressure. Finally, the resultant residue was purified by silica gel column chromatography using ethyl acetate and hexane (1:15, v/v) as eluents to afford **TA-DF-BDM** as yellow solid powder (0.2206 g, 69.7%, m.p.166.2-168.6 oC, $C_{57}H_{59}N_3$: C 87.13, H 7.51, N 5.35; found: C 87.23, H 7.53, N 5.27).

^{1}H NMR (600 MHz, CDCl3) δ 8.02 (d, *J* = 8.4 Hz, 2H), 7.85 (t, *J* = 8.3 Hz, 2H), 7.81 (t, *J* = 3.9 Hz, 2H), 7.78 (d, *J* = 7.9 Hz, 1H), 7.65 (dd, *J* = 7.9, 1.7 Hz, 1H), 7.62-7.54 (m, 5H), 7.31-7.26 (m, 4H), 7.17 (ddd, *J* = 9.7, 7.6, 1.5 Hz, 6H), 7.07-7.03 (m, 2H), 2.04 (dd, *J* = 9.7, 6.8 Hz, 4H), 1.19-1.02 (m, 20H), 0.78 (t, *J* = 7.2 Hz, 6H), 0.72-0.64 (m, 4H).

^{1}H NMR and ^{13}C NMR spectra performed on Bruker DRX 600 spectrometer where tetramethylsilane was used as internal reference for chloroform deuteride. The crystal was kept at 293.41(10) K during data collection. Using Olex2, the structure was solved with the SHELXS structure solution program using Direct Methods and refined with the SHELXL refinement package using Least Squares minimization. Ultraviolet-visible (UV-Vis) absorption and photoluminescence (PL) spectra were recorded on Hitachi U-3900 and Horiba Fluoromax-4 spectrophotometer, respectively. Furthermore, transient fluorescence and low temperature phosphorescence spectra were measured by Edinburgh FLS 980 spectrometer with 365 nm Xenon laser source. Thermal gravimetric analysis (TGA) curves were recorded on a Netzsch TG 209 F3 at a heating rate of 10 ℃/min from 40 to 800 ℃ under nitrogen flow.

The ^{1}H NMR spectrum of M_1, M_2, **TA-DF-BDM** as shown in the **Fig. S1, Fig. S2, Fig. S3,** respectively.

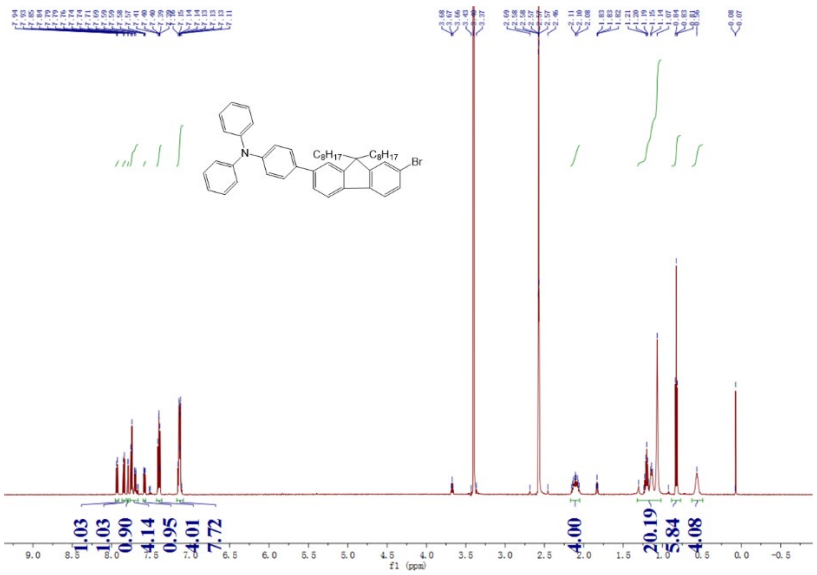

Fig. S1 ^{1}H NMR spectr of M1

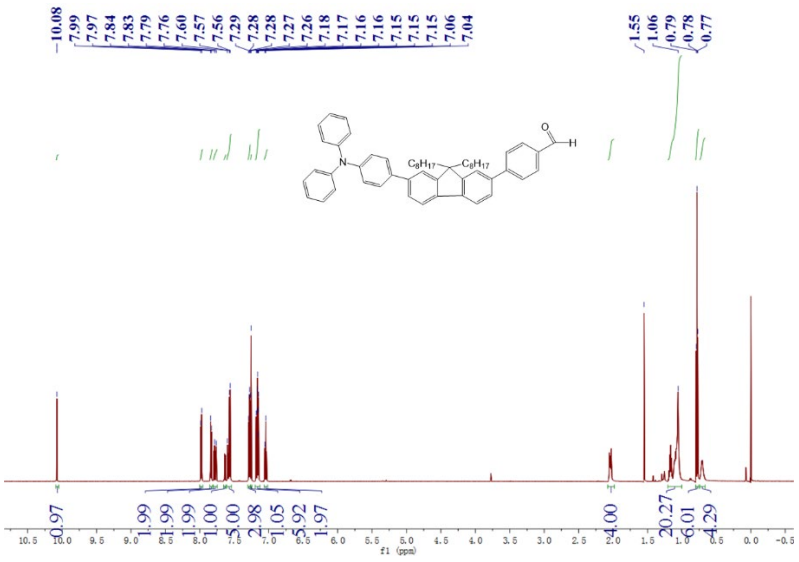

Fig. S2 ^{1}H NMR spectrum of M2

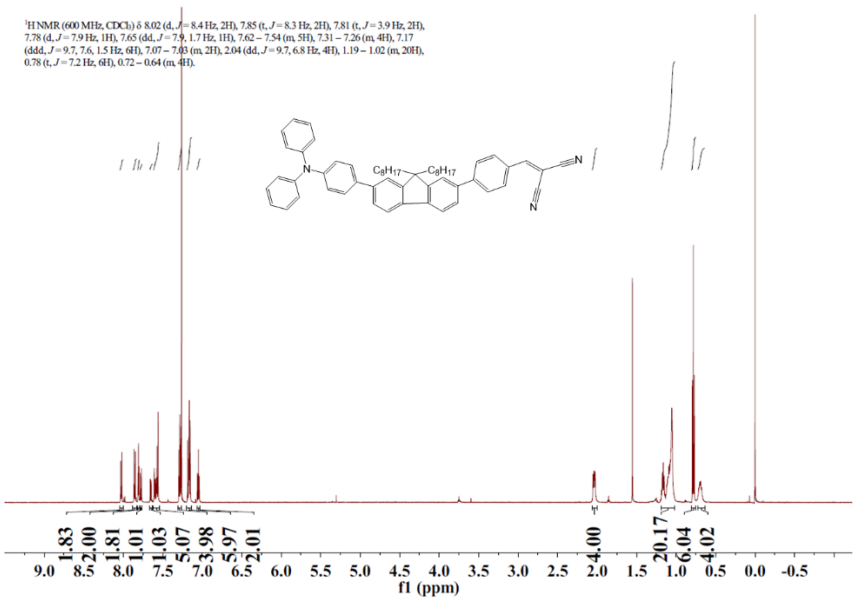

Fig. S3 ^{1}H NMR spectrum of **TA-DF-BDM**

The ^{13}C NMR spectrum of TA-DF-BDM in $CDCl_3$ as shown in the **Figure S4**.

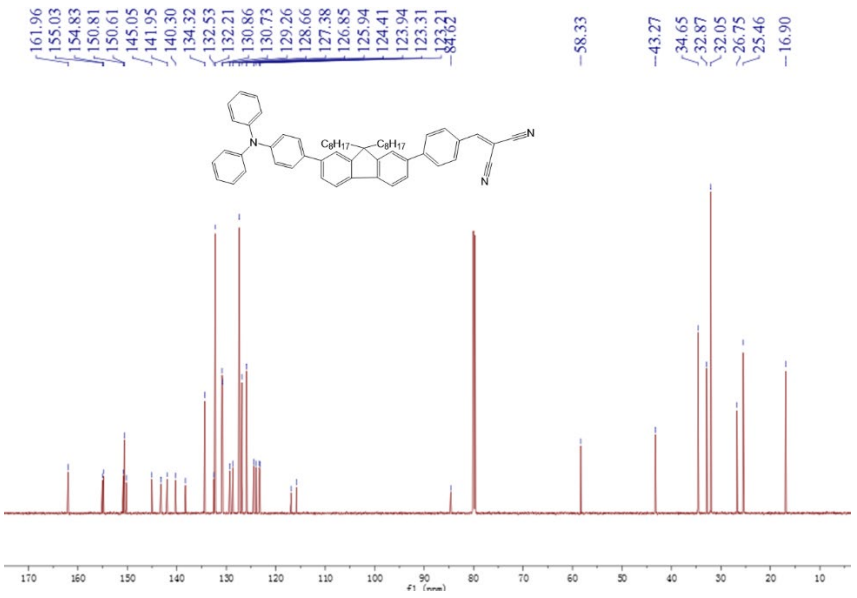

Fig. S4 ^{13}C NMR spectrum of **TA-DF-BDM** in $CDCl_3$

The elemental composition of the M1 and M2 as shown in **Figure S5 and Figure S6.**

Elemental Composition

Parameters	
Tolerance:	±5.00 ppm
Electron:	Odd/Even
Charge:	+1
DBE:	-1.5 - 200.0

Elements Set 1:

Symbol	C	H	N	O	Na	S	Cl	Br
Min	0	0	0	0	0	0	0	1
Max	120	120	3	6	0	0	0	1

Symbol	F	Si	P	B
Min	0	0	0	0
Max	0	0	0	0

Results

Mass	Intensity	Intensity [%]	Formula	Calculated Mass	Mass Difference [mDa]	Mass Difference [ppm]	DBE
712.34842	684.29	6.38	C44 H57 O3 Br	712.34856	-0.14	-0.19	16.0
			C42 H55 N3 O2 Br	712.34722	1.21	1.69	16.5
			C47 H55 N Br	712.35124	-2.82	-3.95	20.5

Fig. S5 The elemental composition of the M1

Elemental Composition

Parameters	
Tolerance:	±5.00 ppm
Electron:	Odd/Even
Charge:	+1
DBE:	-1.5 - 200.0

Elements Set 1:

Symbol	C	H	N	O	Na	S	Cl	Br
Min	0	0	0	0	0	0	0	0
Max	120	120	3	6	0	0	0	0

Symbol	F	Si	P	B
Min	0	0	0	0
Max	0	0	0	0

Results

Mass	Intensity	Intensity [%]	Formula	Calculated Mass	Mass Difference [mDa]	Mass Difference [ppm]	DBE
738.46448	557.19	4.26	C51 H62 O4	738.46426	0.22	0.30	21.0
			C49 H60 N3 O3	738.46292	1.56	2.12	21.5
			C54 H60 N O	738.46694	-2.46	-3.33	25.5

Fig. S6 The elemental composition of the M2

The high resolution ESI-mass spectrum of **TA-DF–BDM** as shown in **Figure S7.**

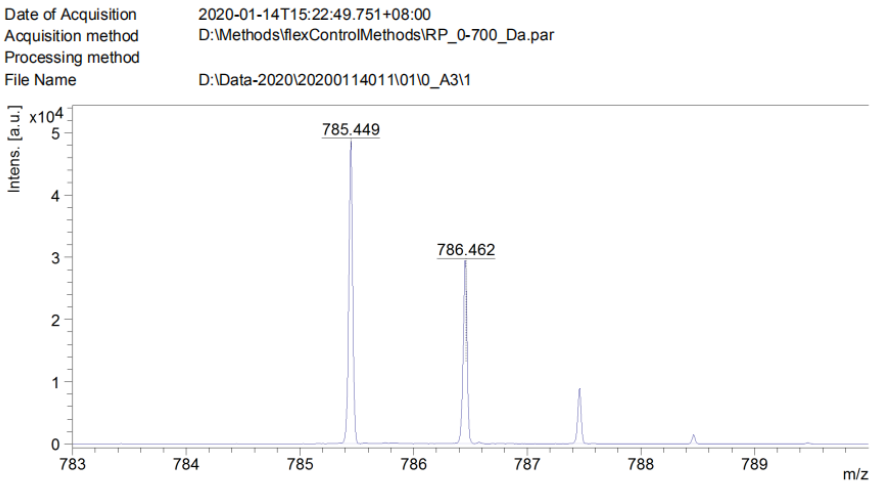

Fig. S7 HRMS spectrum of **TA-DF-BDM**

Section 2. Thermal Properties

The thermal stabilities were investigated by TGA and DSC under a nitrogen atmosphere. As shown in Figure S8, the material TA-DF-BDM performed obvious thermal stability with decomposition temperature (Td) of 413 ℃, and glass transition temperature (Tg) could not be observed, which is originated from the rigid frameworks of the fluorene. The excellent thermal stability of TPA-DFCP is beneficial to the application in OLEDs.

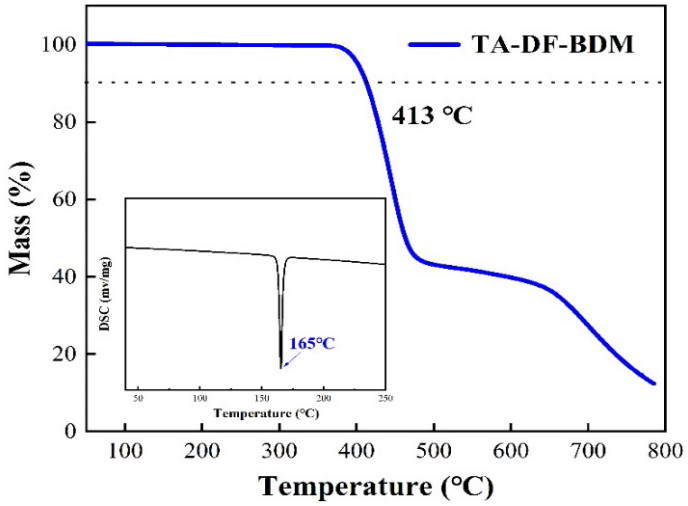

Fig. S8 TGA curve and DSC curve of **TA-DF-BDM**.

Section 3. Single crystal X-ray diffraction data

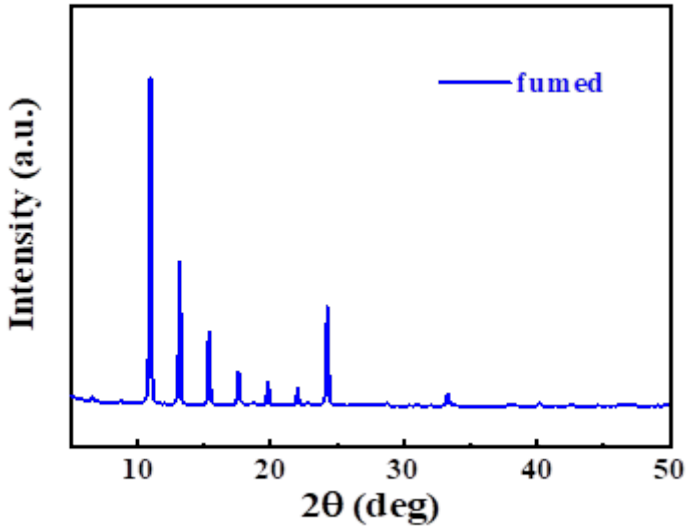

Fig. S9 XRD patterns of **TA-DF-BDM** in fumed solids

Table. 1 Crystal data for TA-DF-BDM

Identification code	TA-DF-BDM
Empirical formula	$C_{57}H_{59}N_3$
Formula weight	786.0700
Temperature/K	293.0000(2)
Crystal system	Triclinic
Space group	P-1
a/Å	10.1571(3)
b/Å	11.4252(5)
c/Å	40.6122(12)
α/°	85.8290(3)
β/°	84.4680(2)
γ/°	89.6460(3)
Volume/Å^3	4678.5000(3)
Z	4.0000
ρ_{calc}g/cm^3	1.1160
μ/mm^{-1}	0.4860
F(000)	1688.0000
Crystal size/mm^3	0.21 × 0.14 × 0.12
Radiation	CuKα (λ = 1.54184)
2θ range for data collection/°	7.7580 to 133.1960
Index ranges	$-12 \le h \le 9$, $-13 \le k \le 13$, $-48 \le l \le 46$
Reflections collected	36256.0000
Independent reflections	15984 [R_{int} = 0.0450, R_{sigma} = 0.0598]
Data/restraints/parameters	15984/72/1085
Goodness-of-fit on F^2	1.0380
Final R indexes [I>=2σ (I)]	R_1 = 0.0733, wR_2 = 0.1941
Final R indexes [all data]	R_1 = 0.1180, wR_2 = 0.2362
Largest diff. peak/hole / e Å^{-3}	0.4400/-0.3400

Section 4. Electroluminescence Performances

We fabricated non-doped OLED based on TA-DF-BDM as the emissive layer with the following device configuration: ITO/MoO_3 (3 nm)/TAPC (40 nm)/TCTA (10 nm)/TA- DF-BDM (5 nm, 10 nm, 15 nm, 20 nm)/TPBI (50 nm)/LiF (1 nm)/Al.

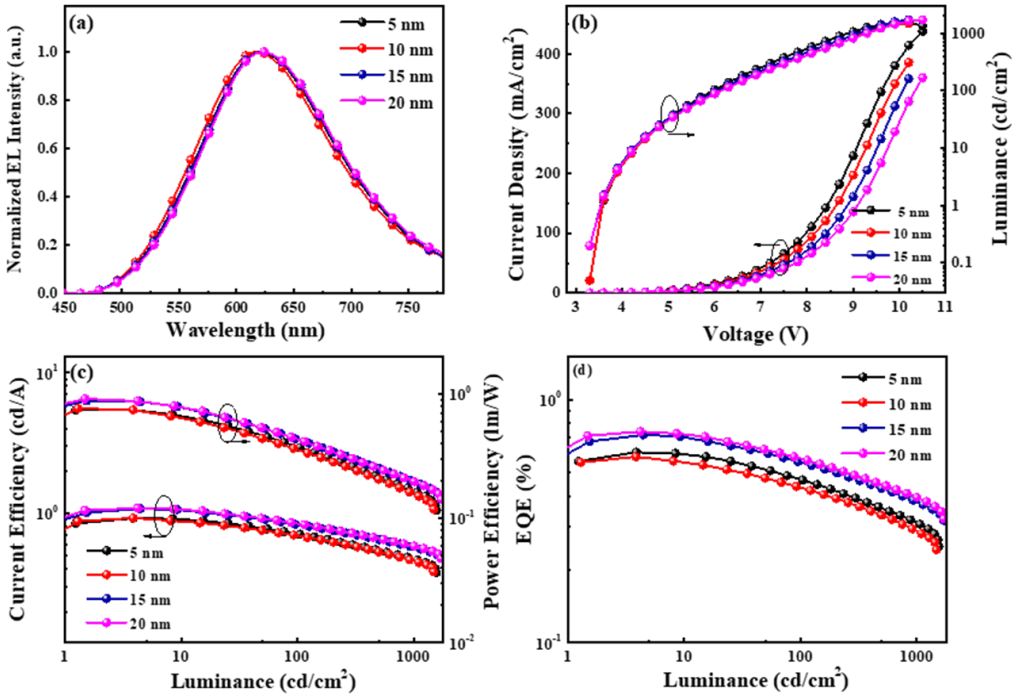

Fig. S 10 EL performance (non-doped) of **TA-DF-BDM**: (a) EL spectra; (b) J-V-L curves; (c) CE-L-PE curves; (d) EQE-L curves

[1] Liu X, Liu W, Wu D, et al.Deep-blue fluorescent emitter based on a 9,9-dioctylfluorene bridge with a hybridized local and charge-transfer excited state for organic light-emitting devices with EQE exceeding 8%, Journal of Materials Chemistry C. DOI: 10.1039/d0tc02941f

[2] Cai M, Zhang D, Huang T, et al. Multifunctional Materials for High-Performance Double-Layer Organic Light-Emitting Diodes: Comparison of Isomers with and without Thermally Activated Delayed Fluorescence. Acs Applied Materials & Interfaces, 2017, 9,17279-17289. DOI: 10.1021/acsami.7b04253

[3] Liu T, Zhu L, Zhong C, et al. Naphthothiadiazole-Based Near-Infrared Emitter with a Photoluminescence Quantum Yield of 60% in Neat Film and External Quantum Efficiencies of up to 3.9% in Nondoped OLEDs, Advanced Functional Materials, 2017, 27(12): 1606384. DOI:10.1002/adfm.201606384

[4] Zhen H, Zhuang J, Xu X, et al. Novel oxazole-based emitters for high efficiency fluorescent OLEDs: Synthesis, characterization, and optoelectronic properties, Tetrahedron, 2017, 73(15): 2036-42. DOI:10.1016/j.tet.2017.02.049

[5] Huang J, Nie H, Zeng J, et al. Highly Efficient Nondoped OLEDs with Negligible Efficiency Roll-Off Fabricated from Aggregation-Induced Delayed Fluorescence Luminogens, Angewandte Chemie, 2017, 56(42):12971-12976. DOI:10.1002/anie.201706752

[6] Yang J, Liu X, Liu Z, et al. Protonation-induced dual fluorescence of a blue fluorescent material with twisted A-π-D-π-A configuration, Journal of Materials Chemistry C, 2020, 8(7): 2442-2450. DOI:10.1039/C9TC06425G

[7] Zeng W, Lai H Y, Lee W K, et al. Achieving Nearly 30% External Quantum Efficiency for Orange–Red Organic Light Emitting Diodes by Employing Thermally Activated Delayed Fluorescence Emitters Composed of 1,8-Naphthalimide-Acridine Hybrids, Advanced Materials, 2018, 30(5): 1704961.1-8. DOI:10.1002/adma.201704961

[8] Seino Y, Inomata S, Sasabe H, et al. High-Performance Green OLEDs Using Thermally Activated Delayed Fluorescence with a Power Efficiency of over 100 lm W-1 [J]. Advanced Materials, 2016, 28(13): 2638-2651. DOI: 10.1002/adma.201503782

[9] Liu K, Xu Z, Yin M. Perylenediimide-cored dendrimers and their bioimaging and gene delivery applications, Progress in Polymer ence, 2015, 46, 25-54. DOI:10.1016/j.progpolymsci.2014.11.005

[10] Xue S, Qiu X, Sun Q, et al. Alkyl length effects on solid-state fluorescence and mechanochromic behavior of small organic luminophores, Journal of Materials Chemistry, C materials for optical and electronic devices, 2016,4 (8), 1568-1578. DOI:10.1039/C5TC04358A

[11] Jiang B, Yu Y, Guo X, et al. White-emitting carbon dots with long alkyl-chain structure: Effective inhibition of aggregation caused quenching effect for label-free imaging of latent fingerprint, Carbon, 2018, 128,12-20. DOI:10.1016/j.carbon.2017.11.070

[12] Lin S, Cheng Y, Lin C, et al. Carbon nanodots with intense emission from green to red and their multifunctional applications, Journal of Alloys and Compounds, 2018, 742, 212-219. DOI:10.1016/j.jallcom.2018.01.194

[13] Luo J, Xie Z, Lam J W Y, et al. Aggregation-induced emission of 1-methyl-1,2,3,4,5-pentaphenylsilole, Chemical Communications, 2001, 18: 1740-1741. DOI:10.1039/B105159H

[14] Dong X, Wang S, Chen G, et al. Synthesis, aggregation-induced emission and thermally activated delayed fluorescence properties of two new compounds based on phenylethene, carbazole and 9,9′,10,10′-tetraoxidethianthrene, Tetrahedron, 2018, 74(4): 497-505. DOI:10.1016/j.tet.2017.12.022

[15] Song F, Xu Z, Zhang Q, et al. Highly Efficient Circularly Polarized Electroluminescence from Aggregation-Induced Emission Luminogens with Amplified Chirality and Delayed Fluorescence, Advanced Functional Materials, 2018, 28(17): 1800051.1-1800051.12. DOI：10.1002/adfm.201800051

[16] Yang J, Huang J, Li Q, et al. Blue AIEgens: approaches to control the intramolecular conjugation and the optimized performance of OLED devices, Journal of Materials Chemistry C, 2016, 4(14): 2663-2684. DOI:10.1039/C5TC03262H

[17] Zhao Z, Gao S, Zheng X, et al. Rational Design of Perylenediimide-Substituted Triphenylethylene to Electron Transporting Aggregation-Induced Emission Luminogens (AIEgens) with High Mobility and Near-Infrared Emission, Advanced Functional Materials, 2018, 28(11): 1705609.1-1705609.1.9. DOI: 10.1002/adfm.201705609

[18] Zhao Z, Nie H, Ge C, et al. Furan is Superior to Thiophene: A Furan-Cored AIEgen with Remarkable Chromism and OLED Performance, Advanced ence, 2017, 4(8): 1700005.1-1700005.8. DOI: 10.1002/advs.201700005

[19] Fan J, Cai L, Lin L, et al. Excited state dynamics for hybridized local and charge transfer state fluorescent emitters with aggregation-induced emission in the solid phase: a QM/MM study, Physical Chemistry Chemical Physics, 2017, 19(44): 29872-29879. DOI:10.1039/c7cp05009g

[20] Tekin E, Smith P J, Hoeppener S, et al. Inside Front Cover: Inkjet Printing of Luminescent CdTe Nanocrystal-Polymer Composites, Advanced Functional Materials, 2007, 17(1): 23. DOI:10.1002/adfm.200790004

[21] Yun S J, Seo M H, Lee S. Dibenzofuran derivatives with meta-and para-triphenylamine substituents as hole-transporting materials in organic light-emitting devices, Dyes & Pigments, 2019, 175:108121. DOI:10.1016/j.dyepig.2019.108121

[22] Zhu Q, Krystyn Van Vliet, Niels Holten-Andersen, et al. A Double-Layer Mechanochromic Hydrogel with Multidirectional Force Sensing and Encryption Capability, Advanced Functional Materials, 2019, 180819.1-180819.8. DOI:10.1002/adfm.201808191

[23] Karvounis A, Aspiotis N, Zeimpekis I, et al. Mechanochromic Reconfigurable Metasurfaces, Advanced ence, 2019, 6(21): 1900974.1-1900974.7. DOI:10.1002/advs.201900974

[24] Vidavsky Y, Yang S J, Abel B A, et al. Enabling Room-Temperature Mechanochromic Activation in a Glassy Polymer: Synthesis and Characterization of Spiropyran Polycarbonate, Journal of the American Chemical Society, 2019, 141(25): 10060–10067. DOI:10.1021/jacs.9b04229